Localized post-buckling states of axially compressed cylinders and their energy barriers

Rainer M. J. Groh* and Alberto Pirrera†
University of Bristol, Queen's Building, University Walk, Bristol, BS1 8TR, UK

The buckling of axially compressed cylinders remains an interesting problem in the engineering mechanics literature. Here we revisit the problem by considering fully localized buckling modes in the form of a single dimple. By applying a combination of nonlinear finite element methods and numerical continuation algorithms, we study the evolution of a single dimple into a ring of circumferential diamond-shaped waves and further into the Yoshimura post-buckling pattern. This post-buckling sequence is established by cellular buckling (homoclinic snaking) as the axial compression is increased; *i.e.* a sequence of de- and restabilizations causes the single dimple to multiply circumferentially. The initial single-dimple seed corresponds to a saddle in the energy landscape, and the energy barrier provided by the single-dimple saddle around the stable pre-buckled path is quantified. The low magnitude of this energy barrier suggests that the pre-buckling equilibrium is metastable once the single dimple exists as a post-buckling equilibrium. We parameterize the onset of metastability with respect to geometric parameters and assess the suitability of this onset as a lower-bound design load. As NASA's well-known lower-bound curve is overly conservative for shells manufactured using modern, tightly-toleranced manufacturing techniques, the onset of metastability could provide a viable and less conservative lower-bound design load.

I. Nomenclature

E = Young's Modulus
F = Axial reaction force
F_c = Classical buckling load $\left(= \frac{2\pi E t^2}{\sqrt{3(1-\nu^2)}}\right)$
$\boldsymbol{f}$ = Internal force vector
$\boldsymbol{F}$ = Force residual
$\boldsymbol{g}$ = Auxiliary equation
$\boldsymbol{G}$ = Extended system
$\boldsymbol{K}_\mathrm{T}$ = Tangential stiffness matrix
L = Cylinder length
N = Arc-length constraint equation
$\boldsymbol{p}$ = External force vector
P = Probe force
R = Cylinder radius
t = Cylinder wall thickness
u = Axial compression (end-shortening)
u_c = Classical buckling displacement $\left(= \frac{1}{\sqrt{3(1-\nu^2)}}\frac{Lt}{R}\right)$
U = Strain energy
$\boldsymbol{u}$ = Displacement vector
w = Radial displacement
$\boldsymbol{y}$ = Vector of unknowns
Z = Batdorf parameter $\left(= \frac{L^2\sqrt{1-\nu^2}}{Rt}\right)$

*Royal Academy of Engineering Research Fellow, Bristol Composites Institute (ACCIS), Dept. of Aerospace Engineering
†Senior Lecturer in Composite Structures & EPSRC Research Fellow, Bristol Composites Institute (ACCIS), Dept. of Aerospace Engineering

δ = Single-dimple imperfection amplitude
η = Non-dimensional buckling parameter
λ = Continuation parameter
$\mathbf{\Lambda}$ = Continuation parameter set
ν = Poisson's ratio
σ_c = Classical buckling stress $\left(= \frac{E}{\sqrt{3(1-\nu^2)}}\frac{t}{R}\right)$
$\boldsymbol{\phi}$ = Critical eigenvector

II. Introduction

The buckling of cylindrical shells is a classic problem in engineering mechanics. Due to the large discrepancy between theoretically predicted and experimentally observed collapse loads, the problem continues to draw attention from researchers. While a linear eigenvalue problem suggests a compressive buckling stress of

$$\sigma_c = \frac{E}{\sqrt{3(1-\nu^2)}}\frac{t}{R}, \tag{1}$$

experimental tests often show collapse loads as low as 20% of this value (E = Young's Modulus, t = shell thickness and ν = Poisson's ratio). Von Kármán & Tsien [1] showed that large deformation equilibrium states exist in the post-buckling regime at much lower values than σ_c. Hence, they attempted to reconcile theory and experiment by suggesting that the knockdown effect occurs as a result of unstable (subcritical) post-buckling behavior with a sharp decrease in load-carrying capacity after the peak load of the classical buckling capacity. The next breakthrough came with Koiter's general theory of elastic stability [2], in which he was able to use an asymptotic approach to quantify the sensitivity of the buckling load with respect to initial imperfections. Due to the sharp unstable post-buckling behavior of the cylinder, initial imperfections round-off the bifurcation point of the idealized shell. These imperfections can take many forms, *e.g.* variations in shell thickness, non-uniform loading, boundary conditions, and geometric imperfections. However, as illustrated by Babcock [3], the greatest contributing factor can be related to the influence of geometric imperfections of the cylinder's mid-surface.

While Koiter's asymptotic approach has been highly successful in predicting knockdown factors for shells with geometric imperfections less than an order of the thickness, the asymptotic approach is less accurate for larger imperfection magnitudes. Furthermore, as pointed out by Zhu *et al.* [4], classical theories fail to account for the nonlinear relationship between the buckling stress (σ_c) and the thickness-to-radius ratio (t/R). While classical theory (see Eq. (1)) suggests a buckling stress proportional to $(t/R)^{1.0}$, empirical data have shown that the stress is actually proportional to $(t/R)^{1.5}$. Zhu *et al.* [4] argue that this discrepancy can be explained by focusing on an inherently imperfect shell—rather than an idealized one with "small" imperfections—where a single dimple is allowed to grow as the applied compression increases. For example, they show that for the case of self-weight buckling of open-topped cylinders, a single post-buckling dimple of a certain size can be held in place by a stress level that is proportional to $t^{1.5}$.

Localizations, such as a single dimple, appear in many structures with subcritical (unstable) post-buckling behavior [6]. As shown in Figure 1, localizations differ from classic (periodic) eigenmodes in that they are confined to a portion of the structure's geometry. Furthermore, localized post-buckling paths can either occur as secondary bifurcations from periodic post-buckling paths, or occur as separate paths in themselves. As shown schematically in Figure 1, the latter case occurs for axially compressed cylinders.

Localizations in the axially compressed cylinder have been the focus of a number of theoretical studies, and more recently, also the topic of experimental work [7]. Using a double-scale asymptotic analysis, Hunt and Lucena Neto [8] showed that post-buckling modes localized along the axial length of the cylinder exist. Hunt *et al.* [9] then showed that one row of this axially localized wave-form can undergo homoclinic snaking as the applied load is varied, thereby adding more and more rings of buckles along the length of the cylinder. Horák *et al.* [5] showed that a single dimple, *i.e.* a post-buckling mode localized both in the axial and circumferential directions, corresponds to a *mountain-pass* point. On an energy landscape, the stable pre-buckled and stable post-buckled equilibria are energy minima separated by a ridge of unstable maxima. The lowest point on this ridge, *i.e.* a saddle in the energy landscape, is a so-called mountain-pass point and provides the lowest energy barrier between the pre-buckled and post-buckled regimes. Because one condition of the mountain-pass algorithm is that the mountain-pass point separates a stable pre-buckling equilibrium from another state with lower energy, the existence of a mountain-pass point implies the "metastability" of the pre-buckling equilibrium.

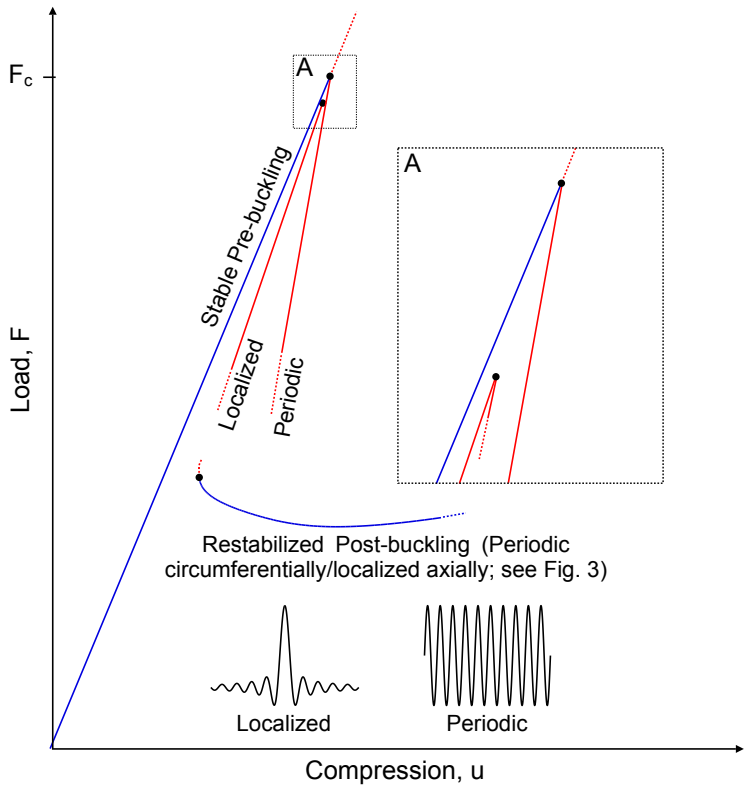

Fig. 1 Schematic load-displacement equilibrium plot of an axially compressed cylinder. The pre-buckling path destabilizes at a symmetry-breaking bifurcation and an unstable post-buckling path of periodic waveform branches from this point. A localized post-buckling mode also exists that does not intersect the pre-buckling path but arises at a limit point (see inset A). As shown by Horák *et al.* [5], localizations, such as a single dimple, represent the smallest energy barrier (saddle in the energy landscape) between the stable pre-buckling and the restabilized post-buckling regimes (two energy wells). Blue segments denote stable equilibria, red segments unstable equilibria, and black dots critical points (limit and bifurcation points).

Hence, once the single-dimple post-buckling mode exists as an equilibrium, the compressed cylinder can transition out of the metastable pre-buckling energy well and into a post-buckling energy well of lower energy. This suggests a possible mechanism for premature buckling via the traversal of small energy barriers surrounding the pre-buckling state. Furthermore, energy barriers of the idealized, perfect shell could, in practice, also be eroded by means of initial imperfections, loading eccentricities, external disturbances or statistical fluctuations, *i.e.* "shocks" [10].

Recently, Kreilos & Schneider [11] showed that for changes in the applied compression, a single dimple undergoes homoclinic snaking in the circumferential direction until the circumference is completely filled with a ring of buckles. Once this ring is complete, snaking in the axial direction, as shown by Hunt *et al.* [9], is possible, although the connection between these two paths could not be established. In this paper, we further examine the stability landscape of an axially compressed cylinder parameterized by a single dimple. We conduct this analysis using nonlinear finite element methods coupled with a numerical continuation solver with branch-switching and bifurcation-tracking capabilities. We show that under variation of the applied compression, the single dimple first grows circumferentially to fill one ring of diamond-shaped buckles around the circumference. Once this sequence is complete, the single ring of diamonds destabilizes at a pitchfork bifurcation, initiating a second and third series of snaking sequences that add further rings along the length of the cylinder. The final shape deep in the post-buckling regime is the well-known Yoshimura pattern [12], observed many times in experiments. By investigating the stability landscape of the cylindrical shell with respect to a lateral side force, the energy barrier separating the stable pre-buckling state from the restabilized post-buckling regime is shown to be an order of magnitude smaller for the single-dimple localization than for a periodic buckling mode, and this energy barrier decays exponentially as end-shortening is increased. Once the single dimple exists as an equilibrium solution, the pre-buckled cylinder is poised in a metastable state from which the cylinder could easily escape through the influence of initial imperfections or external disturbances. Indeed, the onset of metastability is shown to provide a useful lower-bound limit for many experimental buckling loads in the literature.

III. Theory

Due to its versatility, the finite element method is the preferred technique for solving complex problems arising in engineering mechanics. In the applied mathematics community, the mathematical methods of nonlinear multi-parameter analysis, branch switching and bifurcation tracking implemented in numerical continuation codes are well established [13, 14]. These techniques are, however, not classically used for structural mechanics (statics) applications, where specialized arc-length techniques restricted to a single parameter—the applied load—are predominantly used [15, 16]. The application of broader numerical continuation methods within structural finite element solvers often go by the name of "generalized path-following" [17–19], and it is such a framework that we use herein to analyze the stability of the axially compressed cylinder.

The present formulation considers a discretized model of a slowly evolving, conservative and elastic structure, where the internal forces, $\boldsymbol{f}(\boldsymbol{u})$, and tangential stiffness, $\boldsymbol{K}_{\mathrm{T}}(\boldsymbol{u})$, are uniquely defined from the current displacements, $\boldsymbol{u}$, by means of the first and second variations of the total potential energy. Throughout this work, we use so-called "degenerated shell elements" [20], based on the assumptions of first-order shear deformation theory [21] (shear correction factor $k = 5/6$) formulated using the full Green-Lagrange strain tensor and a total Lagrangian reference system. Hence, the analysis allows for finite displacements and rotations but is restricted to the small strains implicit in a classic Hookean constitutive law.

In statics, an equilibrium state is expressed as a balance between internal and external forces, and in a displacement-based finite element setting, this balance is written in terms of n discrete displacement degrees-of-freedom, $\boldsymbol{u}$, and a scalar loading parameter, λ,

$$\boldsymbol{F}(\boldsymbol{u}, \lambda) = \boldsymbol{f}(\boldsymbol{u}) - \boldsymbol{p}(\lambda) = \boldsymbol{0}. \tag{2}$$

The vectors $\boldsymbol{p}(\lambda)$ and $\boldsymbol{f}(\boldsymbol{u})$ are the external (non-follower) load and internal force vector, respectively. In the case of linear and proportional loading we have $\boldsymbol{p}(\lambda) \equiv \lambda \boldsymbol{p}_{,\lambda} = \lambda \hat{\boldsymbol{p}}$, where $\hat{\boldsymbol{p}}$ is a constant reference loading vector (the comma notation is used to denote partial differentiation).

For generalized path-following, Eq. (2) is adapted to incorporate any number of additional parameters, such that,

$$\boldsymbol{F}(\boldsymbol{u}, \boldsymbol{\Lambda}) = \boldsymbol{f}(\boldsymbol{u}, \boldsymbol{\Lambda}_1) - \boldsymbol{p}(\boldsymbol{\Lambda}_2) = \boldsymbol{0}, \tag{3}$$

where $\boldsymbol{\Lambda} = [\boldsymbol{\Lambda}_1^\top, \boldsymbol{\Lambda}_2^\top]^\top = [\lambda_1, \ldots, \lambda_p]^\top$ is a vector containing p control variables, with $\boldsymbol{\Lambda}_1$ corresponding to parameters that influence the internal forces (*e.g.* material properties, geometric dimensions, temperature and moisture fields) and $\boldsymbol{\Lambda}_2$ relating to externally applied mechanical loads (*e.g.* forces, moments and tractions).

The n equilibrium equations in (3) correspond directly to the n displacement degrees of freedom in the system. Because the structural response is parameterized by p additional parameters, a p-dimensional solution manifold in $\mathbb{R}^{(n+p)}$ exists. Specific solution curves on the p-dimensional manifold are defined by incorporating additional equations, $\boldsymbol{g}$. Hence, we wish to evaluate solutions to the extended system

$$\boldsymbol{G}(\boldsymbol{u}, \boldsymbol{\Lambda}) \equiv \begin{pmatrix} \boldsymbol{F}(\boldsymbol{u}, \boldsymbol{\Lambda}) \\ \boldsymbol{g}(\boldsymbol{u}, \boldsymbol{\Lambda}) \end{pmatrix} = \boldsymbol{0}. \tag{4}$$

For r auxiliary equations, the solution to Eq. (4) becomes $(p - r)$-dimensional, and hence $r = p - 1$ auxiliary equations are required to define a one-dimensional curve on the multi-dimensional solution manifold. These curves can describe fundamental equilibrium paths (fundamental loading parameter is varied); parametric equilibrium paths (a non-load parameter is varied); branch-connecting paths that determine the total number of additional branches emanating from a bifurcation point; paths that track bifurcations in parameter space; *etc*. To track bifurcations, for example, the extended system needs to include a criticality condition, *e.g.* $\boldsymbol{g} = \boldsymbol{F}_{,\boldsymbol{u}}\boldsymbol{\phi} \equiv \boldsymbol{K}_{\mathrm{T}}\boldsymbol{\phi} = \boldsymbol{0}$, where $\boldsymbol{\phi}$ is a critical eigenvector associated with a zero eigenvalue. Thus, in the most general form, a vector of q auxiliary variables, $\boldsymbol{v}$, is added to the auxiliary equations $\boldsymbol{g}$,

$$\boldsymbol{G}(\boldsymbol{u}, \boldsymbol{\Lambda}, \boldsymbol{v}) \equiv \begin{pmatrix} \boldsymbol{F}(\boldsymbol{u}, \boldsymbol{\Lambda}) \\ \boldsymbol{g}(\boldsymbol{u}, \boldsymbol{\Lambda}, \boldsymbol{v}) \end{pmatrix} = \boldsymbol{0}. \tag{5}$$

Hence, Eq. (5) describes n equilibrium equations and r auxiliary equations in $(n + p + q)$ unknowns leading to a $(p + q - r)$-dimensional solution. To determine a curve of singular points, we thus require $r = p + q - 1$ auxiliary equations. Following the criticality example for bifurcation tracking referenced above, when the n-dimensional null vector at the critical state is introduced as the auxiliary variable, $\boldsymbol{v}$, a singular curve in two parameters, $p = 2$, is appropriately constrained by the associated $r = n + 1$ auxiliary equations $\boldsymbol{K}_{\mathrm{T}}\boldsymbol{v} = \boldsymbol{0}$ and $||\boldsymbol{v}||_2 = 1$.

When evaluating one-dimensional curves, one additional equation is needed to uniquely constrain the system to a solution point $\boldsymbol{y} = (\boldsymbol{u}, \boldsymbol{\Lambda}, \boldsymbol{v})$. Hence,

$$\boldsymbol{G}^N(\boldsymbol{y}) \equiv \begin{pmatrix} \boldsymbol{F}(\boldsymbol{u}, \boldsymbol{\Lambda}) \\ \boldsymbol{g}(\boldsymbol{u}, \boldsymbol{\Lambda}, \boldsymbol{v}) \\ N(\boldsymbol{u}, \boldsymbol{\Lambda}) \end{pmatrix} = \boldsymbol{0}, \tag{6}$$

where N is a scalar equation which plays the role of a multi-dimensional arc-length constraint. A specific solution to Eq. (6) is determined by a consistent linearization coupled with a Newton's method,

$$\boldsymbol{y}_k^{j+1} = \boldsymbol{y}_k^j - \left(\boldsymbol{G}^N_{,\boldsymbol{y}}(\boldsymbol{y}_k^j)\right)^{-1} \boldsymbol{G}^N(\boldsymbol{y}_k^j) \equiv \boldsymbol{y}_k^j + \delta\boldsymbol{y}_k^j, \tag{7}$$

where the superscript denotes the j^{th} equilibrium iteration and the subscript denotes the k^{th} load increment. The iterative correction cycle is typically started by a predictive forward Euler step.

Within this framework, any arbitrary solution curve can be traced on the equilibrium manifold, as long as a pertinent auxiliary equation, $\boldsymbol{g}$, is defined that constrains the equilibrium equation to the locus of points required. In this particular study we are interested in classic load-displacement curves with one varying parameter, where critical points (bifurcation and limit points) are automatically pinpointed while path-following. Additionally, we compute bifurcation-tracking curves that trace the evolution of a critical point with respect to two parameters. For implementation-specific details on the modeling framework the interested reader is directed to a previous publication [19].

IV. Model

The cylinder modeled here corresponds to the longest cylinder tested in the experiments by Yamaki [22] with $t = 0.247\,\mathrm{mm}$, $R = 100\,\mathrm{mm}$, $L = 160.9\,\mathrm{mm}$, $\nu = 0.3\,\mathrm{mm}$, and $E = 5.56\,\mathrm{GPa}$. The same cylinder was previously considered in many numerical studies, such as the papers by Hunt *et al.* [9] and Kreilos & Schneider [11]. To simulate a physical test condition, both ends of the cylinder are clamped, but one end is free to move axially to impart compression via displacement control (rigid loading).

To reduce the computational effort, and due to the inherent symmetries of the system, only a quarter of the cylinder is modeled here. Imposing symmetry conditions significantly reduces the number of symmetry-breaking bifurcations that can be encountered. Although this curtails the stability landscape, it makes the analysis considerably more manageable. As will be seen, even with the applied symmetry conditions, the observed stability landscape is sufficiently rich.

Throughout the analysis the quarter-cylinder is discretized into a mesh of 121 circumferential and 52 axial nodes for a total of 680 fully integrated 16-node, total Lagrangian shell elements (two rotations per node, no drilling around the shell director). The effects of shear and membrane locking are minimized by using bi-cubic isoparametric interpolation functions (16-node elements). The chosen mesh was refined sufficiently until the first 25 eigenvalues and eigenvectors converged with respect to a 300×77 (circumferential×axial) element mesh of the full cylinder using reduced integration S4R elements of the commercial finite element software Abaqus.

V. Results

The analysis involves two fundamental parameters. The first is the applied end compression (u) and the second a lateral probing force (P) acting at right angles to the cylinder mid-surface, half-way along the cylinder length. The application of this lateral force is used to probe the resilience of the pre-buckled state to lateral disturbances.

As the cylinder is probed from the side for low levels of axial compression, there is a nonlinear softening/stiffening relationship between the probe force (P) and the dimple displacement (w), tracing a sigmoidal equilibrium curve. This curve is drawn in Figure 2(a), where blue segments denote stable equilibria, red segments denote unstable equilibria and black dots denote stability points (bifurcation and limit points). As the axial compression (u) increases, this softening/stiffening behavior becomes more pronounced leading to a segment of negative stiffness. In this case, a lateral probe force would lead to a small pop as the dimple suddenly increases in size across the unstable region. As the axial compression increases further, the load reduces sufficiently on the unstable portion of the curve to pass through the zero load axis ($P = 0$). At this point an additional equilibrium state in the shape of a single dimple has been found. Because the tangential stiffness at this point has one negative eigenvalue, this equilibrium corresponds to a multi-dimensional saddle in the energy landscape. Within a specific range of axial end-shortening, the probing curve re-emerges through the $P = 0$-axis in the form of a stable dimple. However, if the axial compression is increased beyond a threshold, the single dimple no longer exists as a stable equilibrium.

Once a self-equilibrated single-dimple solution is found, *i.e.* an equilibrium solution for vanishing probe force ($P = 0$), the probing force can be removed by definition, and the axial compression increased/decreased to trace the equilibrium curve of the single dimple. Figure 2(b) shows this curve alongside the pre-buckling curve in terms of applied axial compression (u) *vs* transverse displacement (w) of the node at the crest of the dimple. The point where the dimple solution reaches a minimum corresponds to the smallest possible compression for which a single dimple is possible ($u > 1.2 \times 10^{-4}$). Beyond this point, a snaking sequence commences, which will be further discussed in Figure 3. Figure 2(b) also includes an orthographic projection of the locus of limit points on the probing curves shown previously in Figure 2(a). When viewing Figure 2(a)–(b) in aggregate, an interesting stability diagram emerges (see Figure 2(c)) that qualitatively matches the experimental results on a different cylinder by Virot *et al.* [7].

The single-dimple saddle forms an energy barrier between stable pre-buckling states and the restabilized post-buckling regime, and this energy barrier is quantified by the area underneath the probing load *vs* probing displacement curves of Figure 2(a). The energy barrier is intuitively represented by the black ridge (limit point curve) in Figure 2(c), which shows its erosion as compression increases. The energy barrier is quantitatively described in Figure 2(d) as the percentage difference between the strain energy of the pre-buckled state and the strain energy in the single-dimple mode, with these energies calculated for the same level of axial compression. For comparison, the percentage difference between the strain energy of the pre-buckled state and the strain energy of a classic, unstable (subcritical) periodic post-buckling mode emanating from the first bifurcation point on the pre-buckling path is also shown (*i.e.* the mode corresponding to the periodic path in Figure 1). It is clear from Figure 2(d) that the energy barrier of the single dimple is typically an order of magnitude smaller than the energy barrier provided by the periodic mode. This is not surprising as the localized dimple deforms considerably less of the cylinder wall than the periodic mode. Second, the percentage difference between the pre-buckling state and the single dimple is less 0.5% over the range of compression for which the single-dimple solution exists ($u > 1.2 \times 10^{-4}$). How easily this energy barrier is eroded by initial imperfections will be discussed later (see Figure 4), but a general observation is that once the single-dimple localization exists as a post-buckling equilibrium state, the pre-buckling well is "metastable" as it it separated from the post-buckling well of lower energy by only a very small energy barrier.

Figure 3(a) shows equilibrium curves of applied axial compression (u) *vs* axial reaction force (F) for the pre-buckling and dimpled post-buckling states (*i.e.* the mode corresponding to the localized path in Figure 1). As axial compression increases from the unloaded state, the shell loses stability at a bifurcation point ($F = 1193\,N$). By probing the cylinder from the side anywhere in the range of $F > 619$ N we can find an unstable dimple solution. Once one single-dimple solution is found, the axial compression is increased/decreased to trace the dimpled equilibrium path, *i.e.* how the single

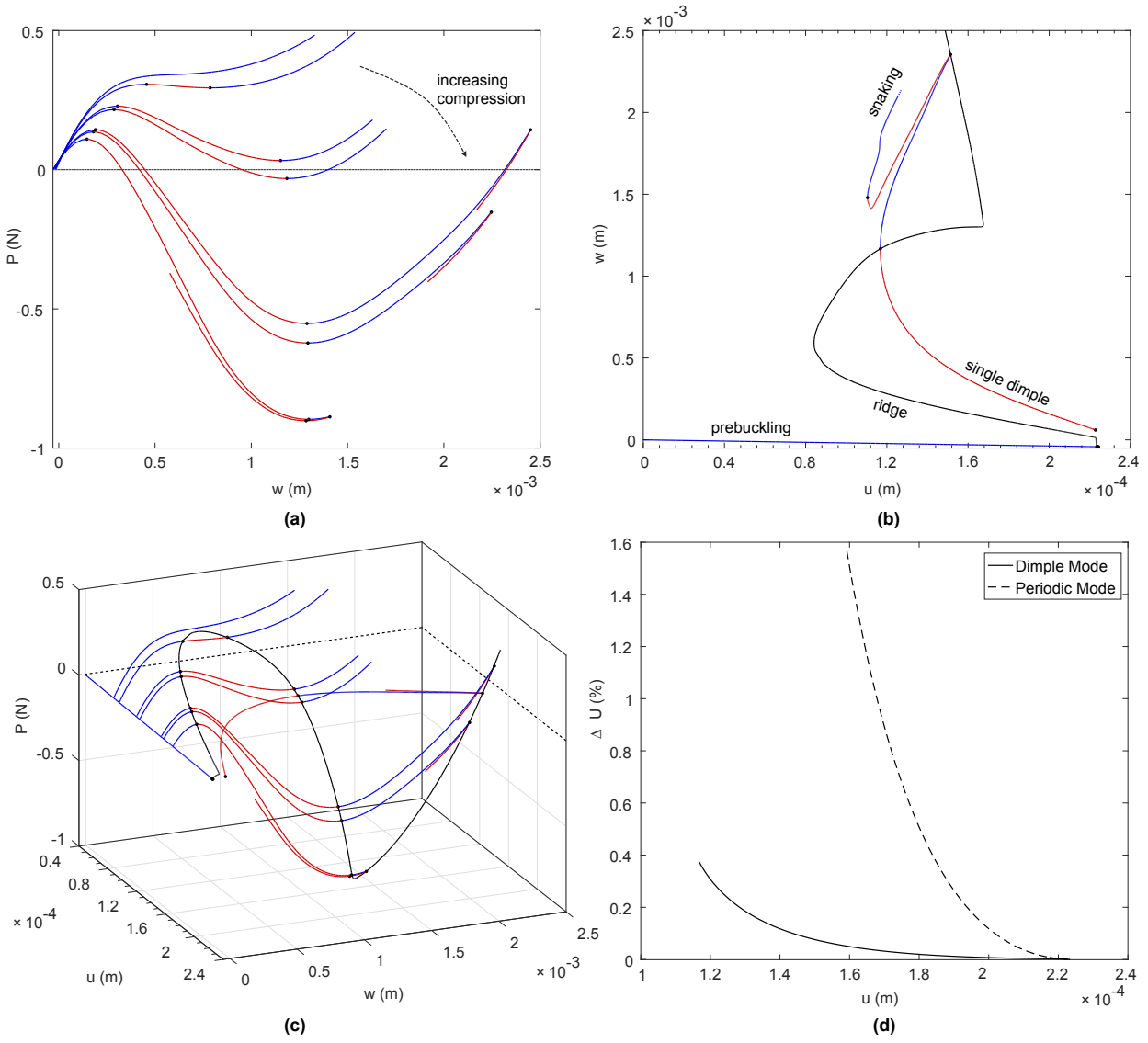

Fig. 2 Stability landscape of an axially compressed cylinder probed by a lateral side load at the cylinder's mid-length (blue is stable, red is unstable, and black dots/lines are critical points). (a) Probe force (P) *vs* probe displacement (w) plots for different values of increasing axial compression (u). The point where $P = 0$ corresponds to a single-dimple equilibrium. (b) Axial compression (u) *vs* probe displacement (w) plot of the pre-buckling and snaking equilibrium paths. The ridge is an orthographic projection of the locus of limit points in (a). (c) A superposition of (a) and (b) showing the full stability landscape in terms of axial compression (u) *vs* probe force (P) *vs* probe displacement (w). (d) The energy barriers (ΔU) around the pre-buckling well formed by the single dimple and a classic periodic post-buckling mode for different levels of applied axial compression (u). The energy barriers are expressed as a percentage difference with respect to the strain energy of the pre-buckled state.

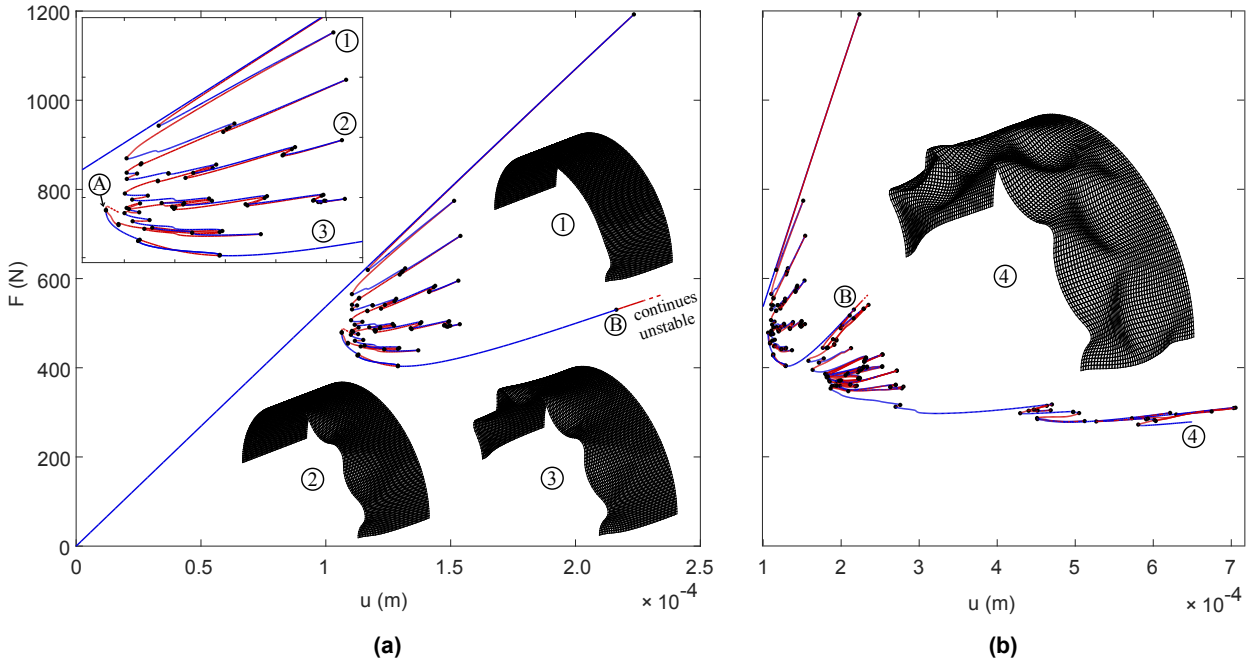

Fig. 3 Equilibrium curves of applied axial compression (u) *vs* axial reaction force (F) for the pre-buckling and dimpled post-buckling states. Statically stable segments are shown in blue, unstable segments in red and critical points (bifurcation and limit points) as black dots. (a) The stable equilibrium path and snaking post-buckling path. On the snaking path, a single dimple grows in a sequence of odd waves until an entire circumferential ring of buckles is filled. At point A (shown in the inset) the snaking curve collides with another curve at a pitchfork bifurcation, which forms the elongated stable (blue) segment corresponding to 10 diamond-shaped buckles. The numbered mode shapes (1, 2 and 3) shown, correspond to the numbered locations in the inset. (b) The localized single ring of buckles destabilizes at bifurcation point B, causing additional series of snaking. Throughout this additional sequence, the end compression increases considerably until the entire cylinder is in a post-buckled shape corresponding to the well-known Yoshimura pattern (see mode shape 4).

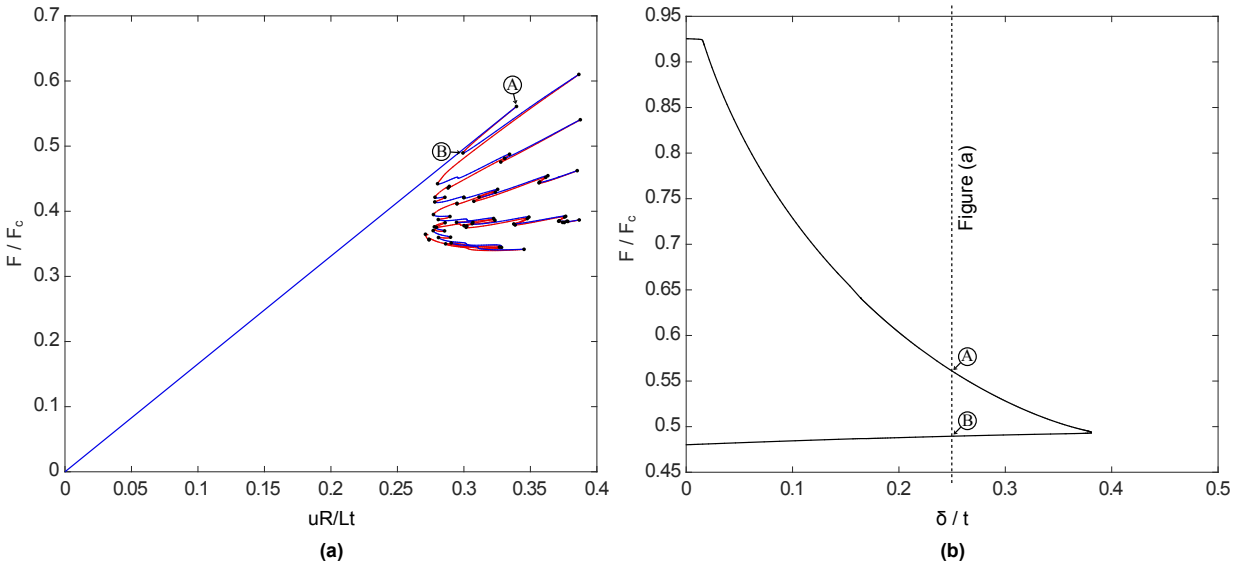

Fig. 4 (a) Equilibrium curve of normalized reaction force F/F_c *vs* normalized displacement uR/Lt of Yamaki's longest cylinder ($Z = 1000$) with a single-dimple imperfection at the mid-length with amplitude (δ) of $0.25\times$ the wall thickness (t). (b) Maximum and minimum limit points (A) and (B) shown in Figure (a) are traced with respect to the imperfection amplitude δ.

dimple evolves with varying end-shortening. As shown in Figure 3(a), the unstable (red) path corresponding to the single dimple is almost indistinguishable from the stable pre-buckling path in blue, indicating the sharp subcritical nature of this buckling mode. With decreasing axial compression, the single dimple stabilizes at a limit point ($u = 0.1168$ mm, $F = 619$ N), which corresponds to a non-dimensional value of $F/F_c = 0.48$, where $F_c = 1290$ N is the classical buckling load derived from Eq. (1). This value of $F/F_c = 0.48$ corresponds exactly to the figure reported previously by Kreilos & Schneider [11].

As the equilibrium path is traced beyond this limit point, the stable single-dimple mode increases in size until it loses stability at a further limit point denoted by point (1) in Figure 3(a). At this point, the dimpled post-buckling curve doubles back on itself and shows the winding path of a homoclinic snaking sequence. The inset in Figure 3(a) shows a feathered equilibrium manifold with five protruding dominant spikes. Each of these spikes corresponds to a unique odd-numbered mode of increasing frequency. As we proceed along the snaking path (in the general direction of decreasing load F), the single dimple grows in the sequence of 1, 3, 5, 7 and 9 waves until an entire ring of buckles around the cylinder is filled. At point A (shown in the inset) the snaking curve takes a total of 10 circumferential waves and collides with another equilibrium path at a pitchfork bifurcation. This additional path forms the elongated stable (blue) segment corresponding to the 10 diamond-shaped buckles depicted by mode shape (3). This 10-diamond mode is axially localized yet circumferentially periodic.

The single row of 10 diamond-shaped buckles then destabilizes at a pitchfork bifurcation (point B). The equilibrium curve emanating from this point is shown in Figure 3(b) and indicates an additional sequence of snaking behavior. Throughout this additional snaking sequence, the end-compression increases considerably until the entire cylinder is in a post-buckled state corresponding to the well-known Yoshimura pattern (see mode (4) in Figure 3(b)). Most experimental studies confirm this wave-form deep in the post-buckling range, and our analysis suggests that it lies on a continuous path beginning from a single dimple as the axial compression is increased.

Previously we suggested that the small energy barrier around the pre-buckling well associated with the single-dimple localization could readily be eroded by initial imperfections. We test this hypothesis by imposing an initial single-dimple imperfection at the cylinder mid-length and loading the cylinder in compression from the unloaded state. The equilibrium path describing the behavior of the cylinder in terms of normalized reaction force F/F_c *vs* normalized displacement uR/Lt is shown in Figure 4(a). This plot corresponds to a single-dimple imperfection amplitude (δ) of $0.25\times$ the wall thickness, *i.e.* $\delta/t = 0.25$. While the idealized perfect cylinder buckled at $F/F_c = 0.925$ (Figure 3(a)), the buckling load of the imperfect cylinder is eroded to $F/F_c = 0.561$, *i.e.* the compressive limit load is eroded by 40% compared to the

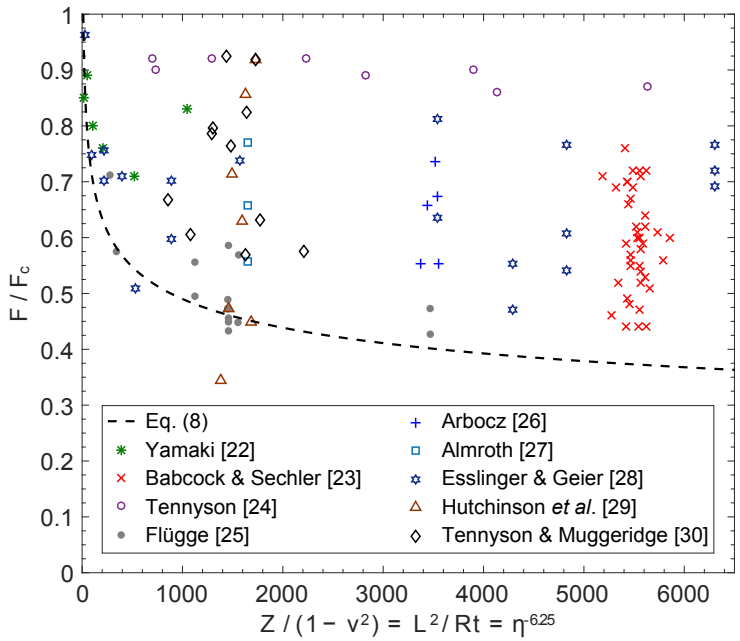

Fig. 5 Critical curve expressed by Eq. (8) **and compared to 115 experimental data points from the literature [22–30].**

idealized perfect cylinder for an imperfection magnitude of only one-quarter of the wall thickness. Furthermore, once buckling commences (point (A) in Figure 4(a)), the cylinder transitions immediately into a localized single-dimple state, which is followed by the previously discussed circumferential snaking sequence. This behavior agrees qualitatively with the evidence reported in most experimental studies in that the buckling process is initiated by a single buckle, which then grows circumferentially (see *e.g* Yamaki [22]). The result of Figure 4(a) thus suggests that the energy barrier of the single-dimple localization is indeed readily eroded by a small imperfection (in this case 25% of the wall thickness).

To quantify the sensitivity of the buckling load with respect to the single-dimple imperfection amplitude, we trace point (A) in Figure 4(a) using the bifurcation-tracking capability. The foldline of limit points in terms of F/F_c *vs* δ/t is shown in Figure 4(b). For no applied imperfection ($\delta/t = 0$), the buckling load of the perfect cylinder is recovered, and as the imperfection is increased, the buckling load drops rapidly. For an imperfection amplitude of $\delta/t = 0.38$, the maximum limit point (A) and minimum limit point (B) collide in a cusp catastrophe, such that beyond the cusp, the cylinder buckles immediately into a three-dimple mode once the pre-buckling path loses stability. At the cusp, the knockdown factor is $F/F_c = 0.49$, and therefore 47% of the buckling load of the idealized perfect cylinder. Thus, the buckling load of this cylinder can be eroded by almost 50% for a single-dimple imperfection of only one-third the wall thickness.

Given that point (B) of the idealized cylinder denotes the lowest value of compression for which the single-dimple localization exists (metastability of the pre-buckling state), we also trace the evolution of this single-dimple limit point with respect to geometric parameters t, R and L. A power-law regression of these foldlines suggests that the end-shortening of the single-dimple limit point varies approximately as $u_{sd} \propto t^{1.16}$, $u_{sd} \propto R^{-0.84}$ and $u_{sd} \propto L^{0.68}$ (to two decimal places with $R^2 > 0.99$ in all three cases). In combination, this regression suggests a critical boundary with respect to the classical prediction ($u_c \propto LtR^{-1}$) of:

$$\frac{u_{sd}}{u_c} = \frac{F}{F_c} = 1.48\frac{R^{0.16}t^{0.16}}{L^{0.32}} = 1.48\eta, \tag{8}$$

where $\eta = R^{0.16}t^{0.16}L^{-0.32}$ is a non-dimensional parameter that describes the onset of metastability of the pre-buckling state. It is striking that there is an apparent power-law relation between the parameter η and the well-known Batdorf geometric parameter Z, *i.e.* $Z/\sqrt{1-\nu^2} = L^2/Rt = \eta^{-6.25}$. The critical boundary expressed by Eq. (8) is drawn on a plot of F/F_c *vs* $\eta^{-6.25}$ in Figure 5 alongside a set of 115 experimental data points taken from nine different studies in the literature [22–30].

Figure 5 shows that the experimental data points fall on or above the metastability curve of Eq. (8) with the exception of one outlier from the study by Hutchinson *et al.* [29]. Many of the studies listed are efforts from the 1960s and 1970s that explicitly set out to manufacture cylindrical shells with geometric tolerances as "nearly perfect as possible" [22–24, 26]. For these cases, the experimental buckling load can be seen to fall well above the critical boundary of metastability. The set of data points also include studies with engineered imperfections [23, 29, 30]. In most cases, the data points of these imperfect cylinders also fall above the metastability curve. Hutchinson *et al.* [29] imposed local axisymmetric imperfections (a localized ridge all around the cylinder circumference) and all data points but one—corresponding to the maximum imperfection amplitude of 73% the wall thickness—are bounded from below by the knockdown curve. Axisymmetric imperfections are known to cause the greatest erosions in buckling load [31], but represent engineered imperfections that are unlikely to occur naturally.

It has been argued [32] that the well-known lower-bound curve of NASA's SP-8007 guideline [33] is overly conservative for shells manufactured using modern manufacturing techniques. NASA's empirical lower-bound curve falls below the dashed curve of Figure 5, and hence, many experimental results from the early 20th century exist below the threshold of Eq. (8). However, many of these studies relied on manufacturing technology much less developed than technology available today. If the geometry can be closely controlled, the onset of metastability as denoted by Eq. (8) could thus provide a viable and less conservative lower-bound design load.

VI. Conclusion

In this paper we have revisited the problem of cylinder buckling from the perspective of fully localized buckling modes in the shape of a single dimple. Using nonlinear quasi-static finite element methods and numerical continuation algorithms we trace the evolution of a single dimple into an axially localized and circumferentially periodic ring of 10 diamond buckles. Furthermore, the single ring of diamond buckles destabilizes at a pitchfork bifurcation, initiating the formation of additional rings of buckles that culminate in the well-known Yoshimura pattern.

As shown by Horák *et al.* [5] the single-dimple localization is a mountain-pass point in the energy landscape that forms the smallest energy barrier between the pre-buckling and post-buckling regimes. This energy barrier is so small that it could easily be eroded by initial imperfections or external disturbances, and hence, initiate premature buckling of the cylinder. Thus, once the single dimple exists as an equilibrium solution for a specific amount of end-shortening, the cylinder is poised in a metastable state. Indeed, initial imperfections in the form of a single dimple are shown to cause premature buckling at load levels considerably less than the classical buckling load. For a dimple imperfection amplitude of only 40% of the wall thickness, the buckling load is eroded by 50%.

By tracing the critical point of end-shortening where the single dimple comes into existence, we have established that the onset of metastability scales approximately as a function of the non-dimensional parameter $\eta = R^{0.16}t^{0.16}L^{-0.32}$. Comparisons with more than 100 experimental data points from the literature suggest that the onset of metastability could be a viable and less conservative lower-bound design load than NASA's SP-8007 guideline [33]. Future work will extend the analysis to more imperfection shapes and extend the analysis to orthotropic material properties.

Acknowledgments

RMJG is supported by the Royal Academy of Engineering under the Research Fellowship scheme [Grant No. RF\201718\17178], and AP is supported by the EPSRC as a Research Fellow [Grant No. EP/M013170/1].

Data statement

All data required to reproduce the figures in this paper can be found on the data repository of the University of Bristol via the URL: https://data.bris.ac.uk/data/.

References

[1] von Karman, T., and Tsien, H.-S., "The Buckling of Thin Cylindrical Shells Under Axial Compression," *Journal of Aeronautical Sciences*, Vol. 8, No. 8, 1941, pp. 303–312.

[2] Koiter, W. T., "Over de stabiliteit van het elastisch evenwicht," phdthesis, Delft University of Technology, Delft, The Netherlands, 1945.

[3] Babcock, C. D., "Shell Stability," *ASME Journal of Applied Mechanics*, Vol. 50, 1983, pp. 935–940.

[4] Zhu, E., Mandal, P., and Calladine, C. R., "Buckling of thin cylindrical shells: An attempt to resolve a paradox," *International Journal of Mechanical Sciences*, Vol. 44, No. 8, 2002, pp. 1583–1601.

[5] Horák, J., Lord, G. J., and Peletier, M. A., "Cylinder Buckling: The mountain pass as an organizing center," *SIAM Journal on Applied Mathematics*, Vol. 66, 2006, pp. 1793–1824.

[6] Thompson, J. M. T., and Virgin, L. N., "Spatial chaos and localisation phenomena in nonlinear elasticity," *Physics Letters A*, Vol. 126, No. 8–9, 1988, pp. 491–496.

[7] Virot, E., Kreilos, T., Schneider, T. M., and Rubinstein, S. M., "Stability Landscape of Shell Buckling," *Physical Review Letters*, Vol. 119, 2017, p. 224101.

[8] Hunt, G. W., and Lucena Neto, E., "Localized buckling in long axially-loaded cylindrical shells," *Journal of the Mechanics and Physics of Solids*, Vol. 39, No. 7, 1991, pp. 881–894.

[9] Hunt, G. W., Lord, G. J., and Champneys, A. R., "Homoclinic and heteroclinic orbits underlying the post-buckling of axially-compressed cylindrical shells," *Computer Methods in Applied Mechanics and Engineering*, Vol. 170, No. 3-4, 1999, pp. 239–251.

[10] Thompson, J. M. T., and Sieber, J., "Shock-Sensitivity in Shell-Like Structures: With Simulations of Spherical Shell Buckling," *International Journal of Bifurcation and Chaos*, Vol. 26, No. 2, 2015, p. 1630003.

[11] Kreilos, T., and Schneider, T. M., "Fully localized post-buckling states of cylindrical shells under axial compression," *Proceedings of the Royal Society A: Mathematical, Physical and Engineering Sciences*, Vol. 473, 2017, p. 20170177.

[12] Yoshimura, Y., "On the Mechanism of Buckling of a Circular Shell under Axial Compression," Tech. Rep. 1390, NACA, Washington, DC, USA, 1955.

[13] Keller, H. B., *Lectures on Numerical Method in Bifurcation Problems*, Tata Institute of Fundamental Research, 1986.

[14] Dödel, E. J., Champneys, A. R., Fairgrieve, T. F., Kuznetsov, Y. A., Sandstede, B., and Wang, X., *AUTO 97: Continuation and Bifurcation software for ordinary differential equations (with HomCont)*, 1998.

[15] Riks, E., "An incremental approach to the solution of snapping and buckling problems," *Journal of Solids and Structures*, Vol. 15, 1979, pp. 529–551.

[16] Crisfield, M. A., "A fast incremental/iterative solution procedure that handles "snap-through"," *Computers and Structures*, Vol. 13, 1981, pp. 55–62.

[17] Rheinboldt, W. C., *Numerical analysis of parameterized nonlinear equations*, 1st ed., Volume 1 of The University of Arkansas Lecture Notes in the Mathematical Sciences, Wiley-Blackwell, 1986.

[18] Eriksson, A., "Structural instability analyses based on generalised path-following," *Computer Methods in Applied Mechanics and Engineering*, Vol. 156, 1998, pp. 45–74.

[19] Groh, R. M. J., Avitabile, D., and Pirrera, A., "Generalised path-following for well-behaved nonlinear structures," *Computer Methods in Applied Mechanics and Engineering*, Vol. 331, 2018, pp. 394–426.

[20] Ahmad, S., Irons, B. M., and Zienkiewicz, O. C., "Analysis of thick and thin shell structures by curved finite elements," *International Journal for Numerical Methods in Engineering*, Vol. 2, 1970, pp. 419–451.

[21] Reissner, E., "On the theory of bending of elastic plates," *Journal of Mathematics and Physics*, Vol. 23, 1944, pp. 184–191.

[22] Yamaki, N., *Elastic stability of circular cylindrical shells*, Elsevier, 1984.

[23] Babcock, C. D., and Sechler, E. E., "The effect of initial imperfections on the buckling stress of cylindrical shells," Tech. Rep. NASA TN D-2005, California Institute of Technology, 1963.

[24] Tennyson, R. C., "Buckling modes of circular cylindrical shells under axial compression," *AIAA Journal*, Vol. 7, 1969, pp. 1481–1487.

[25] Flügge, W., "Die Stabilität der Kreiszylinderschale," *Ingenieur-Archiv*, Vol. 3, 1932, pp. 463–506.

[26] Arbocz, J., "The effect of general imperfections on the buckling of cylindrical shells," Ph.D. thesis, California Institute of Technology, Pasadena, California, USA, 1968.

[27] Almroth, B. O., "Influence of Imperfections and Edge Restraint on the Buckling of Axially Compressed Cylinders," Tech. rep., Lockheed Missiles and Space Company, 1966.

[28] Eßlinger, M., and Geier, B., "Gerechnete Nachbeullasten als untere Grenze der experimentellen axialen Beullasten von Kreiszylindern," *Der Stahlbau*, Vol. 41, No. 12, 1972, pp. 353–360.

[29] Hutchinson, J. W., Tennyson, R. C., and Muggeridge, D. B., "Effect of a local axisymmetric imperfection on the buckling behavior of a circular cylindrical shell under axial compression," *AIAA Journal*, Vol. 9, 1971, pp. 48–52.

[30] Tennyson, R. C., and Muggeridge, D. B., "Buckling of axisymmetric imperfect circular cylindrical shells under axial compression," *AIAA Journal*, Vol. 7, 1969, pp. 2127–2131.

[31] Koiter, W. T., "The Effect of Axisymmetric Imperfections on the Buckling of Cylindrical Shells under Axial Compression," , 1963.

[32] Hühne, C., Rolfes, R., Breitbach, E., and Teßler, J., "Robust design of composite cylindrical shells under axial compression — Simulation and validation," *Thin-Walled Structures*, Vol. 46, 2008, pp. 947–962.

[33] Peterson, J. P., Seide, P., and Weingarten, V. I., "NASA-SP-8007: Buckling of thin-walled circular cylinders," Tech. rep., NASA Langley Research Center; Hampton, VA, USA, 1965.